Attitude Control by Magnetic Torquer

Article *in* Advances in the Astronautical Sciences · January 2009

CITATIONS
11

READS
7,498

2 authors:

Kikuko Miyata
Meijo University
73 PUBLICATIONS **192** CITATIONS
SEE PROFILE

Jozef C. Van der Ha
Satellite Mission Design and Operations
121 PUBLICATIONS **824** CITATIONS
SEE PROFILE

AAS 09-169

ATTITUDE CONTROL BY MAGNETIC TORQUER

Kikuko Miyata* **and Jozef C. van der Ha***

One of the most effective ways for performing low-cost attitude control of satellites is by utilizing the Earth's magnetic-field. In this paper, we present attitude control techniques that use only magnetic devices for active control. First, we summarize a few methods that have been used in orbit. Next, we discuss the details of the control methods. As a concrete example, we select a 50-kg class university satellite, which has three-axis magnetic torquers as the main control equipment. In addition, it has an extension boom that helps attitude stabilization by means of the gravity-gradient effect. We divide the operation period into three main phases corresponding to the expected attitude conditions. We construct a few effective attitude control methods and evaluate control performances on the basis of the results of detailed simulations. Finally, we present details of the development and calibration of magnetic torquers.

INTRODUCTION

During the last 50 years, the importance of satellites in our daily life has been increasing. Because of the importance of satellite missions, new technologies are rarely used in large operational satellites that fulfill critical missions because of fear of failures. In addition, these large satellites tend to be complicated and need a long development period. During the last decade, the development of small and low-cost satellites has become popular. The advantages of small satellites are short development time, design simplicity and lower losses in case of failures. Moreover, small satellites can be launched as sub-payloads so they have a lower launch cost and have many launch opportunities. In order to demonstrate new technologies and to improve the skills of young people, many companies and educational institutes are now developing small satellites. For the development of low-cost satellites, many research efforts are needed. One of these efforts is the pursuit of a low-cost attitude control system. University students look for attitude control equipment that they can design and produce by themselves. For a LEO (Low Earth Orbit) satellite, the most attractive and effective low-cost attitude control techniques is provided by the use of magnetic torquers utilizing the Earth's magnetic field.

These magnetic torquers are fabricated by rolling a conducting wire in the shape of a coil. When a current flows through the wire, it generates the control torque through the interaction with the geomagnetic field. Magnetic torquers are straightforward in design, are very cheap to produce, and are extremely reliable in operations. Moreover, they are light-weight, and consume little electric power. Thus, magnetic torquers have important advantages compared with other actuators.

* Kyushu University, Department of Aeronautics and Astronautics, Space Systems Dynamics Laboratory, 744 Motooka, Nishi-ku, Fukuoka 819-0395, Japan.

In this paper, we focus on the attitude control by magnetic torquer. After the summary of past achievements, we present the design of a small satellite control system as an example. This includes the development and testing of magnetic torquers.

SUMMARY OF PAST SATELLITES

The first report of the use of magnetic field for satellite attitude control was given in the 1960s[1]. Since then, many institutes have considered the use of magnetic control for satellites. With the recent popularity of small satellites, the number of these types of satellites has increased. In this paper, we select some characteristic satellites and discuss their control performances. We focus on satellites using magnetic control during actual on-orbit operations.

The Danish Ørsted satellite[2] was launched on 23 February 1999. This is the first known satellite that uses only the magnetic field for active attitude control. Its total mass is 62 [kg] and its size is 600×450×300 [mm]. It achieves active three-axis stabilization by three sets of magnetic torquers (the total number of torquer coils is 6) with the help of the 8 [m] extension boom's gravity-gradient effect. The attitude control and determination algorithms are re-configurable in real time. The satellite has three control modes depending on the mission phase: the rate de-tumbling control mode, the science observation control mode, and the inverted boom control mode. The first two have successfully been tested in space. However, the third one did not have a chance to be used. The de-tumbling mode uses the B-dot control method with a bias moment that canceled the remnant magnetism. By this method, the satellite can track the local geomagnetic field vector. With the help of the bias moment, the satellite can achieve the required attitude within 5 [deg]. The science control mode uses feedback control based on rates and angles. In this mode, the required attitude is zenith pointing and the angular deviation from the vertical can be achieved within ± 10 [deg] and the yaw attitude within ± 20 [deg].

SNAP-1 (Surrey Nanosatellite Applications Platform)[3] was launched on 28th June 2000 together with the Chinese Tsinghua-1 microsatellite by a Cosmos launch vehicle. Its mass is only 6.5 [kg] and the required attitude is nadir pointing. It has a single pitch momentum wheel and 3-axis magnetorquer rods. After launcher separation, the satellite used the B-dot control and tracked the local geomagnetic field vector. Afterwards, the satellite was switched to the 3-axis stabilization mode. In this mode, the PD control method was used for wheel control and the cross-product method for magnetorquer control. The residual magnetic moment represented the main disturbance torque acting on the satellite. Its magnitude and direction were estimated and the magnetorquer rods were commanded to generate a cancellation moment. By this approach, the nadir pointing performance could be improved to within 3° (1-σ).

The Whale Ecology Observation Satellite (WEOS)[4] was launched on 14th December 2002 as one of the piggy-back satellites on the Japanese H-IIA launcher. This satellite is 50 [cm] cube and its mass is 47.7 [kg]. It has only a one-axis magnetic torquer and a gravity-gradient mast for attitude stabilization. The magnetic torquer and the mast are placed on the upper panel of the satellite. The magnetic torque can generate only two levels, ±1.312 and ±0.656 [ATm^2]. The mast is 3 [m] long and its tip mass is 3 [kg]. The attitude requirement is only rough Earth-pointing. The lower plane always faces to the Earth and the antenna is placed on this surface for communications with the ground station. Just after separation, the satellite was tumbling at the rate of about 0.35 [rpm] for all axes. The de-tumbling control was performed by the B-dot control method. After the conclusion of this mode, the rates had been reduced to about 0.002 [rpm]. The received S-band signal level indicated that the satellite achieved its required rough attitude and that it deployed the mast. After the mast deployment, the satellite achieved rough Earth-pointing and additional attitude control was not performed.

REIMEI[5] is the aurora observation micro-satellite developed by ISAS/JAXA (Institute of Space and Astronautical Science, Japan Exploration Agency). Before launch, this satellite was named INDEX. The satellite configuration is 50 [cm] cube and its mass is about 70 [kg]. It was launched in 2005 by the Russian-Ukrainian launcher as a sub-payload. This satellite has three magnetic torquers and one momentum wheel. The wheel is placed along the roll axis. Initial attitude control is done by only magnetic torquers using a simple control method based on the B-dot control technique. Sun-pointing and spin-stabilization, which make the electric power balanced, were achieved after about 6 hours from separation. Afterwards, the precise attitude control was performed by magnetic torquers and the wheel. In the nominal attitude-control mode, the precision of attitude control is better than 0.5 [deg] and attitude stability is required to be below 0.03 [deg/sec]. The satellite control is based on the feedback control method and the control algorithms are used according to the attitude and mission mode. In addition, this satellite uses also feedforward control based on the remnant magnetism obtained from on-orbit estimation. This approach allowed the cancellation of the effect of the remnant magnetism which is the main disturbance. Because there are significant differences between the on-ground predictions and the on-orbit observations, on-ground measurements data are usually not useful for the feedforward control. This satellite's control system achieved stable inertia pointing with 0.05-0.1 [deg] accuracy.

ATTITUDE CONTROL METHODS

For comparison and evaluation of the control performances of the various methods, we simulate them under identical conditions. In this paper, we use our own small satellite as the control object. After providing an overview of the satellite including its mission, we will introduce the relevant control methods.

Requirements

The satellite under consideration is a 50 [kg] class satellite named "QSAT", which is an abbreviation for "KYUshu SATellite - Polar Plasma Observation Satellite".[6] The satellite configuration is shown in Figure 1. Its size is 480×480×302 [mm]. This satellite is mainly developed by university students. It is a three-axis stabilized satellite which uses only magnetic controller for active control.

QSAT's main mission is to improve our understanding of satellite charging by observations of the electrification of the satellite, the local magnetic field, and the change of plasma density in the auroral zone. This satellite will be launched by the Japanese H-IIA rocket as a piggy-back. The orbit will be circular, sun-synchronous, with an altitude in the range from 600 to 800[km]. Because of the mission requirements, the satellite must keep a rough (*i.e.*, within a few degrees) Earth-pointing attitude.

The satellite has two three-axis sun sensors, two sets of three gyro sensors and two sets of three-axis magnetometers for attitude determination.[7,8] The attitude pointing will be controlled by a set of three magnetic torquers as the only on-board actuators. The three magnetic torquers are oriented along the nominal principal body axes. In addition, QSAT has an extension boom for mission purposes which helps attitude stabilization by the influence of the gravity-gradient effect.

In order to design the necessary attitude control methods, we divide the mission duration into three main phases corresponding to the attitude conditions. The first phase is the de-tumbling phase where the satellite is in a tumbling mode after the separation from the launcher. In this phase, we focus on the reduction of the satellite rotation rates. When the rotation rates are sufficiently low, the extension boom will be deployed. At this time, passive attitude stabilization will be achieved through the gravity-gradient effect because the extended boom will tend to point to the Earth. The third mission phase contains the normal-mode operations. Throughout this phase,

the satellite must be controlled to a rough Earth-pointing attitude. The succession of control phases over the mission is shown in Figure 2.

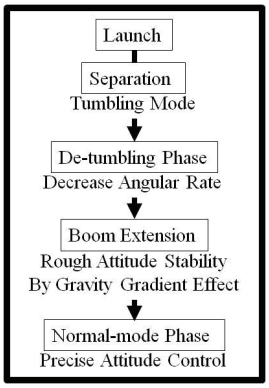

Figure 1. QSAT in Orbit Configuration

Figure 2. Attitude Control Phases

Geometrical Definitions

As shown in Figure 3, the transformation from the inertial axes (***I***,***J***,***K***) to the local orbital axes (x_o,y_o,z_o) is performed by means of the 3-1-3 Euler rotation sequence via the rotation angles (Ω, i, u). In Figure 3, u stands for the argument of latitude and is defined by $u=\omega+f$, with ω the argument of perigee and f the true anomaly. The inclination is given by i and Ω denotes the right ascension of the ascending node.

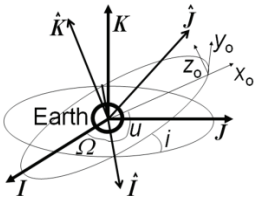

Figure 3. Geocentric Inertial Frame (*I*,*J*,*K*) and Orbital Frame(x_o,y_o,z_o)

The local orbital frame (x_o,y_o,z_o) and the Body-Centered Reference Frame (BCRF) (x_b,y_b,z_b) are shown in Figures. 4-6. The nominal attitude of BCRF is along the orbital reference axes; $x_b=x_o$, $y_b=y_o$, $z_b=z_o$. In this case, the y_b axis is nominally along the velocity direction ***V***.

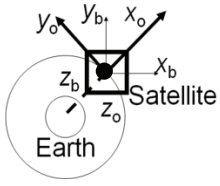

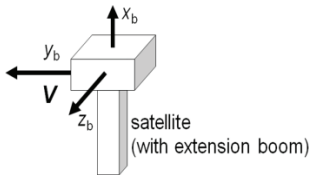

Figure 4. Orbital Frame

Figure 5. Body-Centered Reference Frame (BCRF)

The sequence of transformations from the orbital to the BCRF frame is 3-2-1 via the (ψ,θ,ϕ) angles. As shown in Figures 6, the ψ rotation is along the *z*-axis, the θ rotation is along the *y*-axis, and ϕ is the rotation along the *x*-axis.

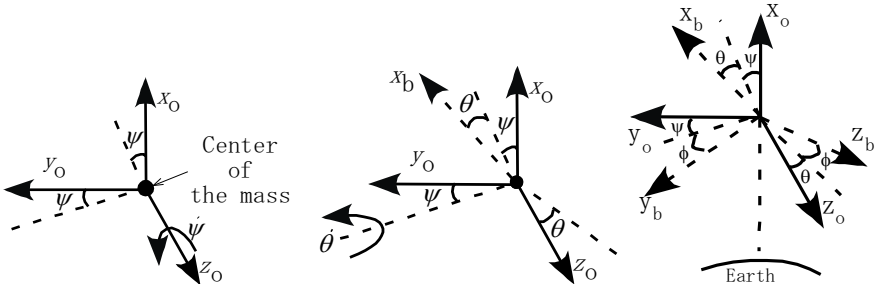

Figure 6. Body Frame to Orbital Frame

B-dot Control Method

In the B-dot control method,[9] the magnetic torquers generate magnetic dipole moments m_i (i=x,y,z) that have the opposite signs of the time variations in the measured geomagnetic field within the spacecraft body frame (dB_i/dt) (i=x,y,z). The generated magnetic moments will be taken equal to the specified maximum values. We define the maximum dipole value as M, so the applied magnetic moment of each magnetic torque m_i can be expressed as:

$$m_i = -M\,\mathrm{sgn}\left(dB_i/dt\right) \quad \left(i = x, y, z\right) \tag{1}$$

As a result, the satellite can reduce its body rates and will eventually align its orientation along a geomagnetic-field line. The satellite achieves its threshold capture energy by the gravity-gradient effect.

PD (Proportional-Derivative) Control Method

This control technique calculates the required control torque components in proportion to the errors in the angles and the angular rates relative to the ideal Earth-pointing orientation and then reduces these errors. The proportionality coefficients between the errors and the required control torques are called the control gains. After introducing the control gains K_x,K_y,K_z,k_x,k_y,k_z, we can calculate the required control torques as:

$$\boldsymbol{T}_c = \begin{bmatrix} T_{cx} \\ T_{cy} \\ T_{cz} \end{bmatrix} = \begin{bmatrix} K_x & 0 & 0 \\ 0 & K_y & 0 \\ 0 & 0 & K_z \end{bmatrix} \begin{bmatrix} \phi \\ \theta \\ \psi \end{bmatrix} + \begin{bmatrix} k_x & 0 & 0 \\ 0 & k_y & 0 \\ 0 & 0 & k_z \end{bmatrix} \begin{bmatrix} \dot{\phi} \\ \dot{\theta} \\ \dot{\psi} \end{bmatrix} \tag{2}$$

In this paper, we calculate the control gains by three different methods; 1) the method based on linearized Euler dynamics equations, 2) the LQR (Linear Quadratic Regulator) method, and 3) the cross-product method which utilizes only magnetometer and rate-gyro sensors measurements data.

However, the required torque cannot be generated in a straightforward manner because the magnetic torquer can only generate a torque vector that is oriented normal to the geomagnetic

vector. Therefore, we need to implement the necessary transformations between the required magnetic torques and the magnetic moments that actually need to be generated.

Method Using Linearized Dynamics

When considering only the gravity-gradient disturbance torque, and assuming short time intervals, small attitude error angles, and neglecting the coupling terms of $(\dot{\phi},\dot{\theta},\dot{\psi})$, the Euler dynamical equations can be expressed as[10]:

$$\begin{aligned} I_x\ddot{\phi} + \omega_o^{\,2}(I_z - I_y)\phi &= T_x \\ I_y\ddot{\theta} - 4\omega_o^{\,2}(I_x - I_z)\theta &= T_y \\ I_z\ddot{\psi} + 3\omega_o^{\,2}(I_y - I_x)\psi &= T_z \end{aligned} \tag{3}$$

Here, ω_o is the orbital rate, $\boldsymbol{T}=\boldsymbol{T}_c+\boldsymbol{T}_d$ with $\boldsymbol{T}_d$ the disturbance torque vector and $\boldsymbol{T}_c$ the control torque vector as defined in Eq. (2). By these relationships, Eqs. (3) can be simplified as:

$$I_i\ddot{\theta}_i + K_i\dot{\theta}_i + c_i\theta_i = T_{di} \quad (i=x,y,z) \tag{4}$$

Here, $\theta_x=\phi$, $\theta_y=\theta$, $\theta_z=\psi$. The additional parameters in Eq. (4) are defined as follows:

$$\begin{aligned} c_x &= (I_z - I_y)\omega_o^{\,2} + K_x \\ c_y &= 4(I_z - I_x)\omega_o^{\,2} + K_y \\ c_z &= 3(I_y - I_x)\omega_o^{\,2} + K_z \end{aligned} \tag{5}$$

In this case, the transfer function of Eq. (4) is:

$$\frac{\Theta_i(s)}{T_{di}(s)} = \frac{1}{I_i s^2 + K_i s + c_i} = \frac{\omega_{ni}^2}{c_i\left(s^2 + 2\zeta_i\omega_{ni}s + \omega_{ni}^2\right)} \quad (i=x,y,z) \tag{6}$$

Here, $\tau_i \equiv K_i/2c_i$, $\omega_{ni} \equiv \sqrt{c_i/I_i}$, $\zeta_i \equiv \tau_i\omega_{ni}$ $(i=x,y,z)$.

From this linearized model, we can calculate the gains using basic linear control theory. We propose the use of the critical damping case with damping ratios $\zeta_i=1$($i=x,y,z$). This represents the limit of rapid response without vibrations. When fixing the control period t_i($i=x,y,z$), the undamped natural frequency is calculated as $\omega_{ni}= 2\pi/t_i$ ($i=x,y,z$) and the time constant is $\tau_i = \zeta_i/\omega_{ni}$ ($i=x,y,z$).

The most suitable control periods t_i ($i=x,y,z$) are determined from the simulation results to be presented below.

From these discussions, we find that the gains are provided by the following equations:

$$\begin{aligned} K_x &= 4\pi^2 I_x / t_x^{\,2} - (I_z - I_y)\omega_o^{\,2} \\ K_y &= 4\pi^2 I_y / t_y^{\,2} - 4(I_z - I_x)\omega_o^{\,2} \\ K_z &= 4\pi^2 I_z / t_z^{\,2} - 3(I_y - I_x)\omega_o^{\,2} \\ k_i &= 16\pi\zeta_i I_i / t_i \quad (i=x,y,z) \end{aligned} \tag{7}$$

LQR (Linear Quadratic Regulator) Method

The LQR (Linear Quadratic Regulator) method[11,12] is a convenient and widely used method to establish the optimal feedback gain of a general linear control system. This theory is concerned with operating a dynamic system at minimum cost. When the system dynamics are described by a set of linear differential equations and the cost is given by a quadratic function we refer to the LQ problem. The LQR method is one of the main results in this theory.

We introduce the state vector $\mathbf{x}=[\phi\ \theta\ \psi\ \omega_x\ \omega_y\ \omega_z\text{-}\omega_o]^T$ and the control torque $\mathbf{u}=[0\ 0\ 0\ T_x\ T_y\ T_z]^T$. In addition, we make use of the fact that $\dot{\Omega}$ is very small compared to $\dot{\phi},\dot{\theta},\dot{\psi},\phi,\theta,\psi$ and we assume no disturbances. The linear state equations can now be expressed in the $\dot{\mathbf{x}}=\mathbf{Ax}+\mathbf{Bu}$ form:

$$\begin{bmatrix}\dot{\phi}\\ \dot{\theta}\\ \dot{\psi}\\ \dot{\omega}_x\\ \dot{\omega}_y\\ \dot{\omega}_z\end{bmatrix}=\begin{bmatrix}0 & \omega_o & 0 & 1 & 0 & 0\\ -\omega_o & 0 & 0 & 0 & 1 & 0\\ 0 & 0 & 0 & 0 & 0 & 1\\ 0 & 0 & 0 & 0 & (I_y-I_z)\omega_o/I_x & 0\\ 0 & 0 & 0 & (I_z-I_x)\omega_o/I_y & 0 & 0\\ 0 & 0 & 0 & 0 & 0 & 0\end{bmatrix}\begin{bmatrix}\phi\\ \theta\\ \psi\\ \omega_x\\ \omega_y\\ \omega_z-\omega_o\end{bmatrix}+\begin{bmatrix}0 & 0 & 0 & 0 & 0 & 0\\ 0 & 0 & 0 & 0 & 0 & 0\\ 0 & 0 & 0 & 0 & 0 & 0\\ 0 & 0 & 0 & 1/I_x & 0 & 0\\ 0 & 0 & 0 & 0 & 1/I_y & 0\\ 0 & 0 & 0 & 0 & 0 & 1/I_z\end{bmatrix}\begin{bmatrix}0\\ 0\\ 0\\ T_{cx}\\ T_{cy}\\ T_{cz}\end{bmatrix} \tag{8}$$

The cost function is defined as:

$$J=\int_0^\infty\left(\mathbf{x}^T\mathbf{Q}\mathbf{x}+\mathbf{u}^T\mathbf{R}\mathbf{u}\right)dt \tag{9}$$

By selecting the appropriate weighting matrices **Q** and **R**, the optimization of the function J balances the energy required for the control and the speed of state vector convergence to 0.

The optimal feedback control gain **K** becomes:

$$\mathbf{u}=-\mathbf{K}\mathbf{x}=-\mathbf{R}^{-1}\mathbf{B}^T\mathbf{P}\mathbf{x} \tag{10}$$

where **P** is found by solving the Riccati equation.

$$\mathbf{A}^T\mathbf{P}+\mathbf{P}\mathbf{A}-\mathbf{P}\mathbf{B}\mathbf{R}^{-1}\mathbf{B}^T\mathbf{P}+\mathbf{Q}=\mathbf{0} \tag{11}$$

The Riccati equation can be solved numerically using MATLAB.

$$\mathbf{P}=\mathbf{Q}+\mathbf{A}^T(\mathbf{P}-\mathbf{P}\mathbf{B}(\mathbf{R}+\mathbf{B}^T\mathbf{P}\mathbf{B})^{-1}\mathbf{B}^T\mathbf{P})\mathbf{A} \tag{12}$$

Cross-Product Method

The Cross-Product method[13] is very attractive for practical in-orbit use because it requires no attitude knowledge. It utilizes only magnetometer and rate gyros measurements. The control performance depends on the measured geomagnetic vector relative to the reference geomagnetic vector. This method does not guarantee that the attitude angles converge to zero because the attitude error in the direction along the geomagnetic field vector cannot be controlled. However, the attitude angles are expected to approach zero over time because the geomagnetic field vector changes its direction continuously in the body frame even when the attitude is in a stable Earth-pointing mode.

This method uses the cross-product vector **c** between the measured geomagnetic vector $\mathbf{b}_m$ in the body frame and the geomagnetic reference vector $\mathbf{b}_r$, predicted by the International Geomag-

netic Reference Field (IGRF) model[14]. When the attitude error angles are small, the direction of **c** becomes essentially the same as the Euler rotation axis for the attitude motion.

The **c** vector is defined as:

$$\boldsymbol{c} = \left(\boldsymbol{b}_m / |\boldsymbol{b}_m|\right) \times \left(\boldsymbol{b}_r / |\boldsymbol{b}_r|\right) \tag{13}$$

After we introduce the error rates $\Delta\boldsymbol{\omega}=[\omega_x \ \omega_y \ \omega_z-\omega_o]^T$ measured by the gyro sensors, we can calculate the required control torque vector $\boldsymbol{T}_R$ from:

$$\boldsymbol{T}_R = [K]\boldsymbol{c} + [k]\Delta\boldsymbol{\omega} \tag{14}$$

$[K]$ and $[k]$ are the gain matrices as shown in Eq. (2). The gains can be calculated as in Eqs. (7) for the case of the linearized dynamics equations. We select the control period from the results of the numerical simulation. The required torque shows a few differences with the results of the previous case because of the different definitions of the error angles and rates.

Calculation of Magnetic Moment from Required Torque

From the required control torque, we must calculate the magnetic moments that the three magnetic torquers must generate. However, there is a fundamental difficulty in using the geomagnetic field for attitude control. The magnetic torque vector always acts in the plane that is normal to the magnetic field vector. Therefore, we must have a strategy for calculating the most suitable magnetic moment vector that can actually be generated and that produces a torque that is as close as possible to the required torque vector.

Here, we present a straightforward but effective procedure for calculating the magnetic moments. The required control torque $\boldsymbol{T}_R$ follows from the control law calculations. Also we have measurements of the magnetic-field vector ($\boldsymbol{B}$) in the body frame from the magnetometer. We introduce the control torque $\boldsymbol{T}_{can}$, which we can actually be generated by the magnetic torquers. Because $\boldsymbol{T}_{can}$ must be normal to the magnetic field, we have $\boldsymbol{B}\cdot\boldsymbol{T}_{can} = 0$. The most efficient magnetic moment is the one that always points normal to the $\boldsymbol{B}$ vector, so that $\boldsymbol{M}\cdot\boldsymbol{T}_{can} = 0$. We know both of the $\boldsymbol{B}$ and $\boldsymbol{T}_R$ vectors and we can calculate $\boldsymbol{T}_{can}$ if we assume that it lies in the plane defined by the vectors $\boldsymbol{B}$ and $\boldsymbol{T}_R$. This assumption makes sense because it minimizes the angle between $\boldsymbol{T}_R$ and $\boldsymbol{T}_{can}$. We define β as the angle between $\boldsymbol{B}$ and $\boldsymbol{T}_R$ (with $0 \le \beta \le \pi$, see Figure 7).

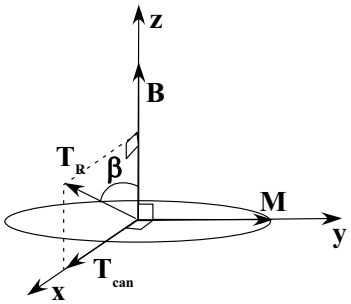

Figure 7. Required Control Torque T_R and Magnetic Moment M

As shown in Figure 7, we introduce the new Cartesian coordinates with the *x* axis along the $\boldsymbol{T}_{can}$ vector, the *y* axis along the magnetic moment vector $\boldsymbol{M}$ and the *z* axis along the $\boldsymbol{B}$ vector.

The respective unit vectors are defined as:

$$\left(\boldsymbol{e}_x, \boldsymbol{e}_y, \boldsymbol{e}_z\right) = \left(\boldsymbol{T}_{can}/T_{can}, \quad \boldsymbol{M}/M, \quad \boldsymbol{B}/B\right) \tag{15}$$

In this case:

$$\boldsymbol{T}_R = \left(T_R \sin\beta\right)\boldsymbol{e}_x + \left(T_R \cos\beta\right)\boldsymbol{e}_z \tag{16}$$

Thus, the $\boldsymbol{T}_{\text{can}}$ vector is:

$$\boldsymbol{T}_{can} = \left(T_R \sin\beta\right)\boldsymbol{e}_x = \boldsymbol{T}_R - \left(T_R \cos\beta\right)\boldsymbol{e}_z = \boldsymbol{T}_R - \left(T_R \cos\beta\right)\boldsymbol{B}/B \tag{17}$$

From the magnetic torquer equation, the torque that can actually be generated, $\boldsymbol{T}_{\text{can}}$, can be described in the form:

$$\boldsymbol{T}_{can} = \boldsymbol{M} \times \boldsymbol{B} \tag{18}$$

When we take the cross product of $\boldsymbol{B}$ with both sides of the above expression, we find:

$$\boldsymbol{B} \times \boldsymbol{T}_{\text{can}} = \boldsymbol{B} \times \left(\boldsymbol{M} \times \boldsymbol{B}\right) = \left(\boldsymbol{B} \bullet \boldsymbol{B}\right)\boldsymbol{M} - \left(\boldsymbol{M} \bullet \boldsymbol{B}\right)\boldsymbol{B} = B^2 \boldsymbol{M} \tag{19}$$

Because the moment $\boldsymbol{M}$ is always applied normal to the $\boldsymbol{B}$-vector, we have $\boldsymbol{M} \cdot \boldsymbol{B} = 0$. From the result in Eq. (19), we obtain:

$$\boldsymbol{M} = \frac{\boldsymbol{B} \times \boldsymbol{T}_{can}}{B^2} \tag{20}$$

From these discussions we can also express the required magnetic moment $\boldsymbol{M}$ in terms of the known field $\boldsymbol{B}$ and the required torque $\boldsymbol{T}_{\text{R}}$ vectors (see Figure 7):

$$\boldsymbol{M} = \frac{\boldsymbol{B} \times \boldsymbol{T}_{can}}{B^2} = \frac{\boldsymbol{B}}{B^2} \times \left\{ \boldsymbol{T}_R - \frac{\left(T_R \cos\beta\right)\boldsymbol{B}}{B} \right\} = \frac{\boldsymbol{B} \times \boldsymbol{T}_R}{B^2} \tag{21}$$

SIMULATIONS

Simulation Conditions

In this section, we present the parameters used in the simulator, the controller performances, the orbital elements, the disturbance torques models, and the conditions at the end of the detumbling phase.

The controllers considered are the magnetic torquers that have been fabricated and tested by ourselves, see Appendix. We design the magnetic moments to generate between + and - 1.3 [Am^2] and we set the operating range as ± 1.0 [Am^2]. In these simulations, the magnetic torquers can generate all values within the range ± 1.0 [Am^2]. In addition, we select the control period as 1 [sec] and the duty ratio as 0.5. (In actual operations, larger intervals may need to be used.)

We assume a circular, sun-synchronous orbit with precession rate $\dot{\Omega} \approx 0.986$ [deg/day] and the orbital elements as in Table 1.

Table 1. Assumed Orbital Elements (Sun-Synchronous Orbit)

i(deg)	Ω(deg)	e	ω(deg)	M(deg)	ω_o(deg/sec)
98.06	105	0.0005	0.001	180	0.061186

Here, i is the inclination, Ω is the right ascension of the ascending node, e is the eccentricity, ω is the argument of perigee, M is the initial mean anomaly, and ω_o is the orbital rate.

For the disturbance torques, we consider the worst-case values of the gravity-gradient torque, the solar radiation pressure torque, the atmospheric drag torque and the remnant magnetic torque.

The gravity-gradient torque is calculated as Eq. (22)[15]:

$$\mathbf{T}_{gg} = \frac{3\mu_E}{R^3}\begin{bmatrix} mn(I_z - I_y) + nlI_{xy} - lmI_{xz} + (n^2 - m^2)I_{yz} \\ nl(I_x - I_z) + lmI_{xy} - mnI_{xy} + (l^2 - n^2)I_{xz} \\ lm(I_y - I_x) + mnI_{xy} - nlI_{yz} + (m^2 - l^2)I_{xy} \end{bmatrix} \tag{22}$$

Here, $\boldsymbol{R}=R(l,m,n)^{\mathrm{T}}$ is the orbital radius vector with origin at the center of the Earth and pointing to the center of mass of the satellite.

The solar radiation pressure torque can be modeled as:

$$\begin{aligned} \mathbf{T}_{srp} &= (\mathbf{c}_{srp} - \mathbf{c}_m) \times \mathbf{F}_{srp} \\ \mathbf{F}_{srp} &= \frac{F_s}{c} A_s (1+q) \mathbf{r}_{sun} \end{aligned} \tag{23}$$

Here, $\mathbf{c}_{srp}$ is the center of solar radiation pressure and $\mathbf{c}_m$ is the center of mass in the BCRF frame. We take 5 [cm] as the distance between $\mathbf{c}_{srp}$ and $\mathbf{c}_m$, which is the worst-case offset. F_s is the solar constant with value 1367.0 [W/m^2], A_s is the effective satellite area, q is the secular reflectivity of the satellite surface for which we choose the worst-case value of 1.0, c is the velocity of light, and $\mathbf{r}_{sun}$ is the unit sun vector as seen in the BCRF frame. The sun direction is calculated using the VSOP87 (Variations Séculaires des Orbites Planétaires) method[16].

The atmospheric drag torque model is given by:

$$\begin{aligned} \mathbf{T}_a &= (\mathbf{c}_a - \mathbf{c}_m) \times \mathbf{F}_a \\ \mathbf{F}_a &= \frac{1}{2} \rho C_d A V \mathbf{V} \end{aligned} \tag{24}$$

Here $\mathbf{c}_a$ is the center of aerodynamic force and the distance between $\mathbf{c}_a$ and $\mathbf{c}_m$ is taken as 5[cm] as was done for the solar radiation pressure torque. C_d is the drag coefficient, ρ is the atmospheric density, and $\mathbf{V}$ is the orbital velocity vector. The atmospheric density is calculated by an exponential model[17].

The remnant magnetic torque can be calculated as:

$$\boldsymbol{T}_{mag} = \boldsymbol{M}_{\boldsymbol{d}} \times \boldsymbol{B} \tag{25}$$

$\boldsymbol{M}_{\mathrm{d}}$ is the effective remnant magnetism of the satellite and its worst-case value is taken as 0.33 [Am^2] which is the maximum acceptable value allowed by the mission requirements. We measure

the remnant magnetism before launch to ensure that it is below the required limit. For simplicity, we assume in the simulation that the on-orbit remnant magnetism is the same as the on-ground measured value. The ***B*** vector is the geomagnetic field vector and is calculated from the IGRF model[14].

For the de-tumbling phase simulations, we use two sets of initial conditions. The first set represents the worst-case value specified by the H-IIA launcher user`s manual[18] where all angular rates are set to 30 [deg/sec]. The other one is taken from the actual observed in-orbit separation rates of WEOS[4] where all angular rates are taken as 2.1[deg/sec] or 0.35 [rpm]. The angles are all set to 0.0 [deg].

Before extension of the boom, the satellite must achieve a rough Earth-pointing attitude. We can use the gravity-gradient torque for assisting of the attitude stabilization once the satellite achieves the rough Earth-pointing attitude. This rough attitude is achieved by the following state (see Reference 4 and Reference 10, p.99):

$$\left|\dot{\phi}_0\right| < \omega_o \frac{\sqrt{(I_y - I_z)I_x}}{I_{x0}},\ \left|\dot{\theta}_0\right| < 2\omega_o \frac{\sqrt{(I_z - I_x)I_y}}{I_{y_0}},\ \left|\dot{\psi}_0\right| < \sqrt{3}\omega_o \frac{\sqrt{(I_y - I_x)I_z}}{I_{z0}} \tag{26}$$

Here, I_x, I_y, I_z are the inertia moments after the boom extension, I_{x0}, I_{y0}, I_{z0} are the inertia moments before boom extension, $\dot{\phi}_0, \dot{\theta}_0, \dot{\psi}_0$ are the required angular variations to maintain the Earth-pointing mode before boom extension and ω_o is the orbital rate.

For normal-mode simulations, the initial angles and rates are set to 0.0 [deg or deg/sec]. This is the ideal condition at the end of the de-tumbling phase. The target angles are 0.0 [deg] and the target rates are 0.0 [deg/sec] except for ω_z, which has the target rate of ω_o [deg/sec].

De-tumbling Simulation Results

In this section, we present the results for the de-tumbling phase and focus on the rate results. In the simulations, we choose two different inertia conditions (after and before the boom extension) and initial conditions (worst-case or realistic satellite conditions). For the worst-case and before boom extension simulations, we used all 4 methods. Next, we show the results for the other conditions only for the best method.

First, we show the results of the B-dot control method. In this method, the signs of the initial conditions and remnant magnetism have no effect on the results. Figure 8 shows the case when all initial conditions and the remnant magnetism have positive signs. In this case, we achieve a rough Earth-pointing attitude after about 8 hours of control effort.

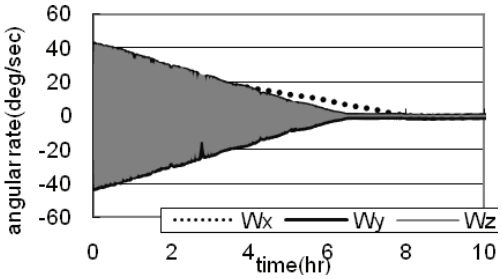

Figure 8. Worst-case B-dot Results before Boom Extension

In the following cases, we assume that the remnant magnetism is roughly known from the on-ground measurements. Therefore, we can negate the remnant magnetic effect by feed-forward control which will continuously be generating magnetic moments that are opposite to the remnant magnetism.

Figure 9 shows the results for the linearized equations method. The signs of the initial conditions and remnant magnetism have no effects on the results in this case either. From the simulations, we find that the best control periods are t ≈ 3200 [sec] for all three axes so we will use this values. Figure 9 shows the case where all initial conditions and the remnant magnetism have positive signs. This method requires about a half hour longer to finish the de-tumbling than the B-dot method.

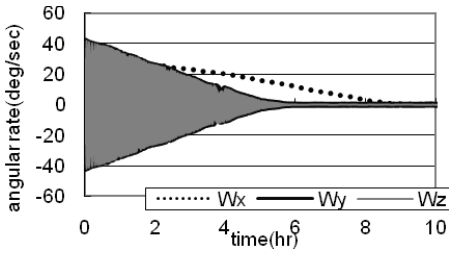

Figure 9. Worst-case Linearized Equation Results before Boom Extension

The results of the LQR method are shown in Figure 10. We use the following weighting matrices in this case. The **Q** matrix has only diagonal terms and these terms are given by:

$$\mathbf{Q} = diag\begin{bmatrix} 8 & 8 & 8 & 1 & 1 & 1 \end{bmatrix} \tag{27}$$

The **R** matrix is the 6 × 6 matrix and can be expressed by the Kronecker delta.

$$\mathbf{R} = 10^{10}\left[\delta_{ij}\right] = \begin{cases} 1.0\times10^{10}\left(i=j\right) \\ 0\left(i\neq j\right) \end{cases} \qquad i,j=1,\ldots,6 \tag{28}$$

The signs of the initial conditions and the presence of the remnant magnetism have almost no effects on this result. Figure 10 shows the case that all initial conditions and signs of the remnant magnetism are positive. The LQR method needs a little longer time to complete the de-tumbling and its computing time is also longer than for the B-dot method.

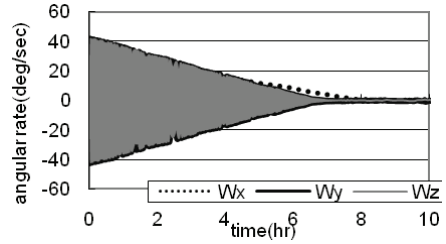

Figure 10. Worst-case LQR Results before Boom Extension

The cross-product method results are shown in Figure 11. As before the signs of the initial conditions and remnant magnetism have little effects on the result. From the simulations, we get the best control periods for $t \approx 2500$ [sec] for all axes and we will use these values. Figure 11 shows the case that all initial conditions and remnant magnetism signs are positive. This case also needs about a half hour more than the B-dot method to finish the de-tumbling.

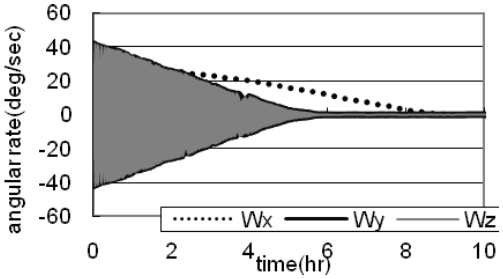

Figure 11. Worst-case Cross Product Results before Boom Extension

Figure 12 shows the B-dot de-tumbling results after the boom extension. The initial conditions are the same as in Figure 8. This case needs about 14 hours to finish the de-tumbling. This result indicates that it is better to perform the boom extension after completion of the rough de-tumbling.

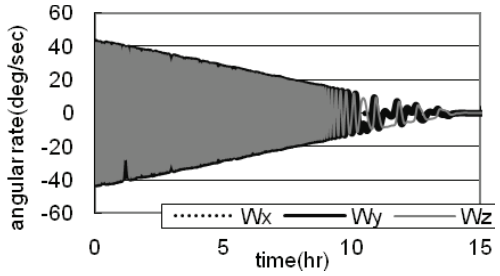

Figure 12. Worst-case B-dot Results after Boom Extension

Figure 13 shows the case with more realistic initial rates. In this case, the de-tumbling operations will be finished within 2 hours when selecting the B-dot method.

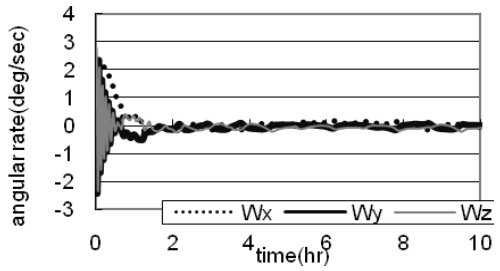

Figure 13. Realistic B-dot Results before Boom Extension

Normal-mode Simulations Results

In this section, we present the results for the rates, angles, as well as generated magnetic moments. The results of the normal-mode simulations are shown for each group of methods. The left-side Figures show the results without disturbance torques, whereas the right-side Figures show the results including the disturbance effects. We also assume that the remnant magnetism is roughly known from the on-ground measurements. Therefore, we can negate the remnant magnetic effect by feed-forward control which will continuously be generating the magnetic moments opposite to the remnant magnetism.

First, we show the results of the linearized equation method in Figures 14 to 16. When there are no disturbances, the best control periods are $t \approx 3200$ [sec] and we can achieve the target values within about 6 hours. In the presence of disturbances, the best control periods are also $t \approx 3200$ [sec] and the trends are roughly the same as without disturbances. However, oscillations caused by the disturbances appear in all results. These oscillations lead to angular errors of about -1.0 to 1.5 [deg]. The largest error appears in the pitch axis.

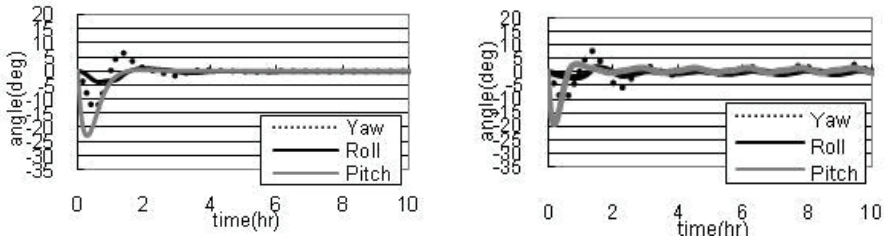

Figure 14. Angles Results of Linearized Equation

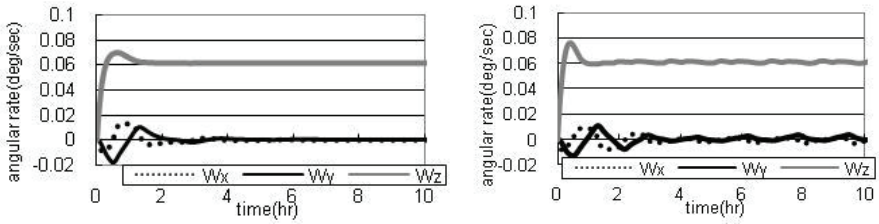

Figure 15. Rates Results of Linearized Equation

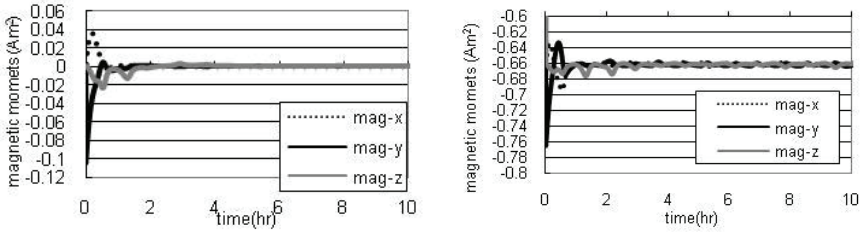

Figure 16. Magnetic Moments Results of Linearized Equation

For the LQR method, we use the following weighting matrices. The **Q** matrix has only diagonal terms and these terms are given by:

$$\mathbf{Q} = diag\begin{bmatrix} 8 & 8 & 8 & 1 & 1 & 1 \end{bmatrix} \tag{29}$$

The **R** matrix is a 6 × 6 matrix and can be expressed by the Kronecker delta. When there are no disturbances, we use left matrix and, in the case when disturbances are taken into account, we use the right matrix from the simulation results.

$$\mathbf{R} = 10^{12}\left[\delta_{ij}\right] = \begin{cases} 1.0\times10^{12}\,(i=j) \\ 0\,(i\neq j) \end{cases}, \qquad \mathbf{R} = 10^{13}\left[\delta_{ij}\right] = \begin{cases} 1.0\times10^{13}\,(i=j) \\ 0\,(i\neq j) \end{cases} \quad i,j=1,\ldots,6 \tag{30}$$

The results of the simulations are shown in Figures 17-19. In the case when there are no disturbances, we can achieve the target values within about 7 hours. The control trends are roughly the same as in the linearized equation case. However, this method provides a much too large control torque for the pitch rate at the beginning. When the disturbance torques are included, the remaining errors become larger than in the linearized equation case.

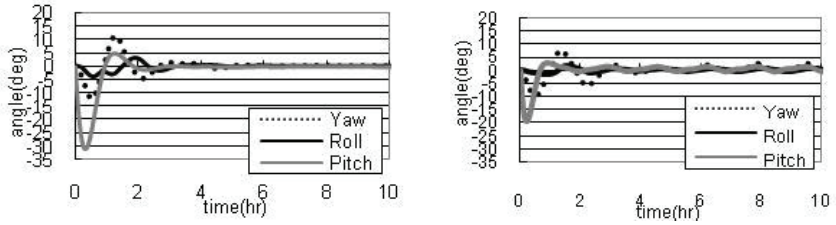

Figure 17. Angles Results of LQR

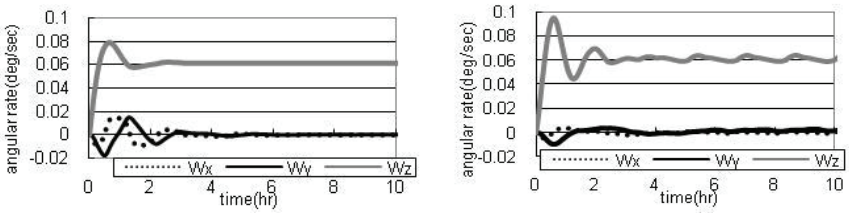

Figure 18. Rates Results of LQR

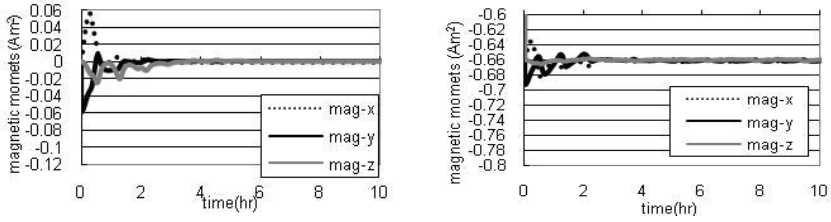

Figure 19. Magnetic Moments Results of LQR

The final results are those produced by the cross-product method shown in Figure 20-22. When there are no disturbances, the best control periods are t ≈ 3000 [sec] and we can achieve the target values within about 16 hours. The results show considerable oscillations. The control performances seem to be worse than for the other methods because of the longer control time and the oscillations in the angles. When the disturbances are included, the best control periods are t ≈ 6000 [sec] and we can achieve the target values within about 15 hours. However, the best control period becomes twice as large as in the no-disturbances case. The difficulty of the gain tuning also becomes a disadvantage.

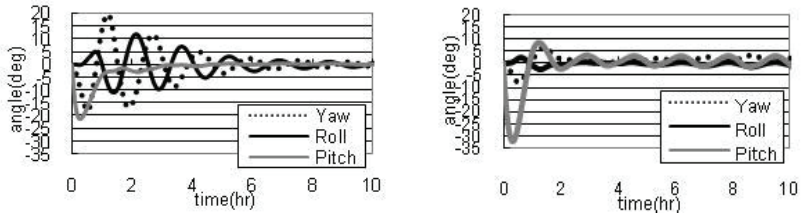

Figure 20. Angles Results of Cross Product

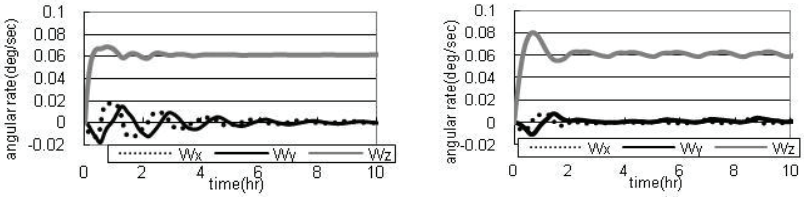

Figure 21. Rates Results of Cross Product

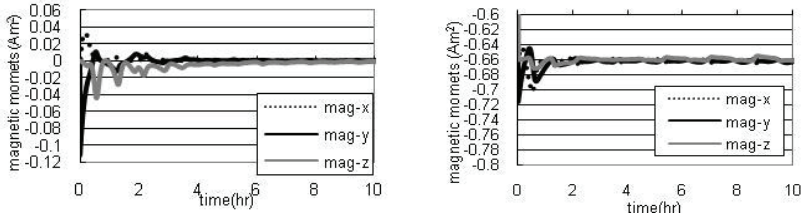

Figure 22. Magnetic Moments Results of Cross Product

CONCLUSION

This paper has demonstrated the usefulness of employing magnetic torques for satellite attitude control. It was found that the control to a rough attitude pointing orientation can be achieved by using only magnetic torques. For more precise control performances, the magnetic control may be combined with the use of a pitch momentum wheel.

The effectiveness of the B-dot control method for the de-tumbling mode has been confirmed by the satellite simulation results. Unlike the other methods, this method does not use lineariza-

tion in gain calculations. For the normal-mode control, it is necessary to determine the remnant magnetism and to negate its effect by applying the opposite magnetic moment using the magnetic torquer.[2-5]

For the evaluation of the control performances, we summarize the parameter errors from the normal-mode simulations for each method and each condition. The error parameters are calculated as the averaged value of the absolute errors from 4 to 5 orbital periods after the start of the control. In the first three rows, the results for the no-disturbance simulations are shown whereas the lower three rows show the results when disturbances are included. The angles are in units of degrees, and the rates are in degree/second. From these results, we conclude that the required rough Earth pointing can adequately be achieved by all methods considered here. The yaw angle shows the largest errors for all methods. The linearized equation method shows good results in the normal-mode simulations. The gains show good robustness against disturbances. One of the reasons of this is that only this method considers the gravity-gradient effect in the gain calculation.

Table 2. Averaged Control Errors

	Method	Yaw	Roll	Pitch	$\sqrt{\Delta\phi^2+\Delta\theta^2+\Delta\psi^2}$	ω_x	ω_y	ω_z
No dis	Linearized Equation	0.0359	0.0177	0.0034	0.0402	5.7×10^{-5}	4.4×10^{-5}	1.4×10^{-5}
	LQR	0.0446	0.0191	0.0069	0.0490	5.6×10^{-5}	5.1×10^{-5}	1.4×10^{-5}
	Cross Product	1.0836	1.0324	0.3610	1.5395	1.0×10^{-3}	1.0×10^{-3}	1.0×10^{-4}
All dis	Linearized Equation	0.9750	0.3992	0.6516	1.2387	1.2×10^{-3}	1.4×10^{-3}	4.4×10^{-4}
	LQR	1.7242	0.2486	1.5663	2.3427	3.2×10^{-4}	1.8×10^{-3}	1.4×10^{-3}
	Cross Product	1.5217	0.4834	1.4003	2.1237	7.7×10^{-4}	1.6×10^{-3}	1.2×10^{-3}

APPENDIX: MAGNETIC TORQUER DESIGN AND PERFORMANCE

The control torque $\boldsymbol{T}$ can be described in terms of the generated magnetic moment **M** and the geomagnetic field **B** as follows:

$$\boldsymbol{T} = \boldsymbol{M} \times \boldsymbol{B} \tag{A1}$$

We can model the theoretical geomagnetic field by means of the model[14] applied to the parameters of the injection orbit. When using a rough estimate of the required control torque, we can decide the required magnetic moments.

Design of Magnetic Torquer

As mentioned in Reference 18, the relationship between the generated magnetic moment m and the control current i can be described as

$$\begin{aligned} m &= \frac{\pi r^2 N}{k_1} i \\ k_1 &= 1/\mu_r + N_d \\ N_d &= \left(d^2/l^2\right)\left(\ell n\left(2l/d\right) - 1\right) \end{aligned} \tag{A2}$$

Here, r is the radius of the magnetic core, N is the turn number of the wire, μ_r is the relative magnetic permeability of the core, N_d is the demagnetization, d is the diameter of the core, and l

is its length. For the calculation of the generated magnetic moment, we have to decide the diameter, length, and material of the core, as well as the material and the turn number of the wire.

At Kyushu University, we are developing magnetic torquers for small satellites. The required magnetic moment is 1.0 [Am^2]. In order to maintain the shape and to reduce the power consumption of magnetic torquers, ferromagnetic cores are chosen. The material is permalloy PB, which is the material name from JIS (Japanese Industrial Standards). It has a high performance and is inexpensive. Its relative magnetic permeability μ_r is 4500. The lengths of the cores are constrained by the dimensions of the main structure of our satellite, because a longer torquer would be more efficient[19]. The wider core diameters are also more efficient. However, the wider core leads to a higher cost and gains in weight. The diameters are decided by the acceptable cost performance and weight efficiency. The material of the wire is selected as WG35 because it is thin and therefore we can use a higher turn number. To increase the turn number as much as possible, the copper wire is reeled in two layers and the turn number is as large as 950. The maximum current applied to the torquers is limited to 0.2 [A], because the permissible current of this copper wire is 0.33 [A].

On the basis of these considerations and the relationships in Eq. (A2), we obtain the specifications summarized in Table A1.

Table A1. Torquer Specifications

Maximum Magnetic Moments	±1.3 [Am^2]
Power	< 0.32[W]
Material of Core Rod	Permalloy PB
Core Length	145 [mm]
Core Diameter	10.4 [mm]
Material of Conducting Wire	Cu (SWG35)
Turn Number	950
Maximum Current	±0.2 [A]

At present, we have already constructed nine torquers based on these design parameters. Before the actual implementation on the satellite, these torquers still need to be calibrated.

Calibration of Torquers

For the torquer calibrations, we determine the relationship between the generated magnetic moment and the applied voltage. By measuring the torque`s resistances, we can calculate the currents from the voltage and the expected generated magnetic moments by Eq. (A2).

The actual generated magnetic moments are calculated by magnetic field measurements. As shown in Figure A1, a magnetometor is placed along the direction of the torquer's long axis. The heights from the ground are set to the same level for the sensor and torquer.

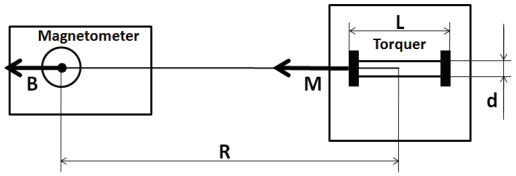

Figure A1. Definition of Variables for the Magnetic Torquer

Here, **M** is the dipole moment of the torquer, **B** is the measured magnetic-flux density, L is the torquer's core length, d is the torquer's core diameter, and R is the distance between the measured magnetic-flux density and the center of the torquer core. In our measurements, we used R =1.2 [m]. With the vacuum permeability $\mu_0=4\pi\times10^{-7}$ [N/A^2] and parameter λ=R/L, the transfer equation between **M** and **B**, can be derived from Eq. (8) in Reference 20 as follows:

$$M = \frac{4\pi}{\mu_0}\frac{\left(\lambda^2 - 1/4\right)^2}{\lambda} L^3 B \tag{A3}$$

We measured the magnetic field of a magnetic torquer in the magnetically shielded room, at ISAS/JAXA. The torquer is placed at the center of the room. In this case, magnetic field variations in the background hardly influence the measurements. We measured the magnetic field of six magnetic torquers with five different applied voltages for each. Figures A2 show one set of the results. The left Figure shows the measured magnetic density results and the right Figure shows the calculated magnetic moments results.

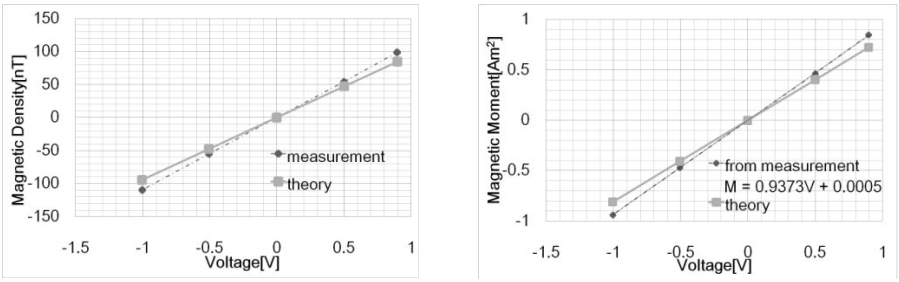

Figure A2. Magnetic Density Measurement (left) and Magnetic Moments Calculation (right)

Figure A2 shows that the measurements have essentially the same linear trend as the theorectical predictions. The differences are proportional to the voltage. As a possibility of the causes of this discrepancy, the difference between the measured and the actual resistance of the circuit may be considered. From the calculations as illustrated on the right of Figure A2, we can calculate the approximate calibration curve. The linear approximations of the calibration curves are of the form:

$$M[\mathrm{Am}^2] = a\mathrm{V}[\mathrm{vol}] + b \tag{A4}$$

The constants *a* and *b* have been established for the 6 magnetic torquer in Table A2.

Table A2. Calibration constants

	1	2	3	4	5	6
a	0.9223	0.9474	0.9522	0.9373	0.9454	0.9472
b	-0.0251	-0.0032	0.0012	0.0005	0.0006	-0.0009

ACKNOWLEDGMENT

We thank Prof. Matsuoka and Mr. Iguchi (from Matsuoka laboratory at ISAS/JAXA) for their assistance during the magnetic measurement tests.

REFERENCES

[1] White, J.S., Shigemoto,F.H., and Bourquin,K., "Satellite attitude control utilizing the Earth's magnetic field." *NASA TND1068*, August, 1961

[2] T. Bak, M. Blanke and R. Wisniewski, "Flight Results and Lessons Learned from the Ørsted Attitude Control Systems." *Proceedings of 4th ESA International Conference on Spacecraft Guidance, Navigation and Control Systems*, ESTEC SP-425, 2000, pp. 87-94

[3] W.H. Steyn and Y. Hashida, "In-orbit Attitude Performance of the 3-Axis Stabilised SNAP-1 Nanosatelllite." *Proceedings of 15th Annual AIAA/USU Conference on Small Satellites*, Utah State University, Logan, USA, 2001, Paper SSC01-V-1

[4] Shigeru Hosokawa, Yoshinari Masumoto, Susumu Takezawa, Kazuhiko Haneji, "Effective Attitude Control System for Small Satellite." *Transactions of the Society of Instrument and Control Engineers (T. SICE)*, Vol.42, No.2, February 2006, pp. 123-128 (in Japanese)

[5] Shin-ichiro Sakai, Yosuke Fukushima and Hirobumi Sait, "Design and On-orbit Evaluation of Attitude Control System for Small Scientific Satellite "REIMEI"." *Proceedings of 25th ISTS (International Symposium on Space Technology and Science)*, Kanazawa, Japan, June 4-11, 2006, Paper 2006-d-84

[6] Yoshihiro Tsuruda, Toshiya Hanada and Jozef van der Ha, "QSAT: A Low-Cost Design for 50kg Class Piggyback Satellite." *Proceedings of 26th International Symposium on Space Technology and Science*, Hamamatsu, Japan, June 2-6 2008, Paper 2008-f-20

[7] Yuya Mimasu and Jozef van der Ha, "Attitude Determination Concept for QSAT." *Proceedings of 26th International Symposium on Space Technology and Science*, Hamamatsu, Japan, June 2-6 2008, Paper 2008-d-13

[8] Yuya Mimasu, Tomohiro Narumi and Jozef van der Ha, "Attitude Determination by Magnetometer and Gyros During Eclipse." *Proceedings of AIAA/AAS Astrodynamics Specialist Conference and Exhibit*, Honolulu, Hawaii, August 20, 2008, Paper AIAA-2008-6932

[9] A. Craig Stickler, K. T. Alfriend, "Elementary Magnetic Attitude Control System." *Journal of Spacecraft and Rockets*, Vol. 13, No.5, 1976, pp. 282

[10] *Spacecraft Attitude Dynamics and Control*, Vladimir A. Chobotov, Orbit, a Foundation Series, Krieger Publishing Company, Original Edition, October 1991

[11] Mark .L. Psiaki, "Magnetic Torquer Attitude Control via Asymptotic Periodic Linear Quadratic Regulation.", *Journal of Guidance, Control, and Dynamics,* Vol. 24, No.2, 2001, pp. 386-394

[12] Rafał Wiśniewski, "Linear Time-Varying Approach to Satellite Attitude Control Using Only Electromagnetic Actuation.", *Journal of Guidance, Control, and Dynamics,* Vol. 23, No.4, 2000, pp. 640-647

[13] W.H. Steyn, Y.Hashida and V.Lappas, "An Attitude Control System and Commissioning Results of the SNAP-1 Nanosatellite." *Proceedings of 14th AIAA/USU Conference on Small Satellites*, Utah State University, Logan, UT, USA, 2000, Paper SSC00-VIII-8.

[14] Nakatsuka, T, "Calculation of the International Geomagnetic Reference Field (4)." *GSJ Open File Report* No. 423, 2005

[15] van der Ha, J., "Model of Gravity Force and Gravity Gradient Torque." *FLK-SIM-TN-ZAR-004 Issue 1*, ZARM, University of Bremen, Germany, April 2006

[16] Meeus, J., *Astronomical Algorithms*, Willmann-Bell, Richmond, Virginia, US, Second Edition, 2005

[17] David A. Vallado, *Fundamentals of Astrodynamics and Applications (The Space Technology Library)*, Springer Scientific + Business Media-Berlin, Third Edition, 2007

[18] *Piggy Back Satellite ,H-IIA Rocket User's Manual*, JAXA

[19] Gregg Radtke, "Technical Note: Magnetic Torquer Overview." *University of Arizona Student Satellite Project*, 1999, Document No. GNC-014, Revision 2

[20] J. Lee, A. Ng and R. Jobanputra, "On Determining Dipole Moments of a Magnetic Torquer Rod Experiments and Discussions." *Canadian Aeronautics and Space Journal*, Vol 48, No. 1, 2002, pp. 61-67.